Author Manuscript

Author Manuscript

Author Manuscript

Author Manuscript

HHS Public Access

Author manuscript

Cell Rep. Author manuscript; available in PMC 2016 June 16.

Published in final edited form as:

Cell Rep. 2015 June 16; 11(10): 1519–1528. doi:10.1016/j.celrep.2015.05.005.

ADAMTS9 mediated extracellular matrix dynamics regulates umbilical cord vascular smooth muscle differentiation and rotation

Sumeda Nandadasa, **Courtney M. Nelson**, and **Suneel S. Apte***

Department of Biomedical Engineering, Cleveland Clinic Lerner Research Institute, Cleveland, OH 44195, United States of America

Summary

Despite the significance for fetal nourishment in mammals, mechanisms of umbilical cord vascular growth remain poorly understood. Here, the secreted metalloprotease ADAMTS9 is shown to be necessary for murine umbilical cord vascular development. Restricting it to the cell-surface using a gene trap allele, *Adamts9*^{Gt}, impaired umbilical vessel elongation and radial growth, via reduced versican proteolysis and accumulation of extracellular matrix (ECM). Both *Adamts9*^{Gt} and conditional *Adamts9* deletion revealed that ADAMTS9 produced by mesenchymal cells acted non-autonomously to regulate smooth muscle cell (SMC) proliferation, differentiation and orthogonal reorientation during growth of the umbilical vasculature. In *Adamts9*^{Gt}, we observed interference with PDGFRβ signaling via the MAPK/ERK pathway, which regulates cytoskeletal dynamics during SMC rotation. In addition, we observed disrupted Shh signaling and perturbed orientation of the mesenchymal primary cilium. Thus, ECM dynamics is a major influence on umbilical vascular SMC fate, with ADAMTS9 acting as its principal mediator.

Introduction

The umbilical cord is the sole fetal-maternal link in placental mammals, conducting blood from the fetus for exchange in the placenta. Excessively long or short cords or cord vascular anomalies, are associated with high fetal morbidity, and a risk of stillbirth (Benirschke K., 2012). Umbilical vessels must remodel extensively after chorio-allantoic fusion, as they grow to accommodate increasing fetal metabolic demand. However, this process has not been studied and little is known about umbilical cord extracellular matrix (ECM) remodeling.

© 2015 Published by Elsevier Inc.

***Corresponding author**: Department of Biomedical Engineering-ND20, Lerner Research Institute, Cleveland Clinic, 9500 Euclid Avenue, Cleveland, OH 44195, USA. aptes@ccf.org; Tel: 216 445-3278; Fax: 216 444-9198 .

Author contributions: S.N. designed and conducted experiments and wrote the manuscript; C.N. conducted experiments, SA designed experiments and wrote the manuscript.

Publisher's Disclaimer: This is a PDF file of an unedited manuscript that has been accepted for publication. As a service to our customers we are providing this early version of the manuscript. The manuscript will undergo copyediting, typesetting, and review of the resulting proof before it is published in its final citable form. Please note that during the production process errors may be discovered which could affect the content, and all legal disclaimers that apply to the journal pertain.

Author Manuscript Author Manuscript Author Manuscript Author Manuscript

ECM comprises networks of collagenous and non-collagenous proteins (Mouw et al., 2014), and is remodeled in all morphogenetic processes, e.g., branching morphogenesis, and sculpting of interdigital webs and heart valves (Bonnans et al., 2014; Dupuis et al., 2011; McCulloch et al., 2009). A pre-gastrulation embryo has a sparse, cell-associated ECM (Kwon et al., 2008; Miner et al., 2004). Later, interstitial ECM expands in mesenchyme, but it is a provisional ECM containing fibronectin (Peters and Hynes, 1996), hyaluronan (Camenisch et al., 2000), and the hyaluronan-binding proteoglycan versican (Naso et al., 1995), and less of mature ECM components such as collagens and elastin. Provisional ECM provides a foothold for cell attachment and is easily remodeled. It gradually transitions to a specialized matrix toward birth, although the umbilical cord, which is not destined for a post-natal life, maintains a proteoglycan-rich matrix named Wharton's jelly (Sobolewski et al., 1997), containing 1-2 arteries and a vein, the whole sheathed in mesothelium.

ADAMTS (A disintegrin-like and metalloprotease with thrombospondin type 1 motifs) proteinases (Apte, 2009) remodel provisional ECM in diverse morphogenetic processes (Dupuis et al., 2011; Enomoto, 2010; McCulloch et al., 2009; Stankunas et al., 2008; Stupka et al., 2013). ADAMTS9 is highly conserved; its *C.elegans* ortholog, Gon-1 is required for gonadal morphogenesis (Blelloch et al., 1999) and the *D. melanogaster* ortholog AdamTS-A is essential for salivary gland morphogenesis and germ cell migration (Ismat et al., 2013). *Adamts9* null mice die at the onset of gastrulation (Enomoto, 2010), but haploinsufficient and conditionally targeted mice identified later developmental roles (Dubail et al., 2014; Enomoto, 2010; Kern et al., 2010). Here, an *Adamts9* gene-trap mutant, where ADAMTS9 is restricted to the cell surface, revealed distinct pools of ADAMTS9 activity, cell-proximal and distal, and requirement of the distal pool for umbilical cord vascular development in mice. ADAMTS9 is thus identified as a crucial component of the pathway connecting ECM dynamics to cellular regulation in this context.

Results and Discussion

An *Adamts9* gene trap generates membrane-anchored ADAMTS9

The $Adamts9^{Gt}$ mouse allele was made from ES cells with UPATrap insertion in intron 30 (Fig.S1A). $Adamts9^{Gt/+}$ mice were externally normal and fertile. Tiled PCR of $Adamts9^{Gt/+}$ genomic DNA identified the UPATrap insertion site (Fig. S1B), allowing genotyping of $Adamts9^{Gt}$ and wild-type (WT) alleles (Fig. S1C).

In $Adamts9^{Gt}$, splicing of exon 30 to the Bcl2α splice acceptor from UPATrap led to a frame-shift in thrombospondin type 1 repeat (TSR) 13, deleted three downstream TSRs and the Gon-1 domain and resulted in a stop codon 44 amino acids downstream (Fig. S1D, Fig. 1A). The new C-terminus, DAFVELYGPSMRPLFDFSWLSLKTLLSLALVGACITLGAYLSHK, matched the C-terminus of human Bcl2α, a mitochondrial membrane protein (transmembrane domain underlined). Thus, $Adamts9^{Gt}$ expressed a C-terminally truncated, constitutively membrane-anchored ADAMTS9 (Fig. 1A). Despite this, $Adamts9^{Gt/Gt}$ embryos underwent gastrulation, and were externally normal until E11.5 (Fig. 1B, Table S1).

Author Manuscript Author Manuscript Author Manuscript Author Manuscript

Expression plasmids for ADAMTS9-GTa and ADAMTS9-GTb, reflecting splice variants affecting TSR11 and TSR12 (GenBank accession: XM_006505260.1, XM_006505263.1) (Fig. S1E-F), and a control construct (ADAMTS9 N-TSR12) were generated (Fig. S2A). We observed localization of ADAMTS9-GTa/b to the secretory pathway and cell membrane (Fig. S2B) but not to mitochondria in transfected COS-1 cells (Fig. S2B). Western blotting consistently showed less cellular ADAMTS9-GT than the control construct in transfected cells, and ADAMTS9-GTa/b were undetectable in the medium (Fig. S2C). Cell-surface biotinylation demonstrated ADAMTS9 N-TSR12 zymogen and a smaller, furin-processed (mature) form (Fig. S2D), which disappeared along with reduction of biotinylated zymogen upon trypsinization, consistent with work showing that ADAMTS9 zymogen bound avidly to the cell-surface, but the mature form did not (Koo et al., 2006, 2007). ADAMTS9-GTa/b were biotinylated and sensitive to trypsin, confirming cell-surface location, but only ADAMTS9-GTa/b zymogen was detected, suggesting lack of furin processing (Fig. S2D). Thus, ADAMTS9-GT was present at lower levels in transfected cells than WT ADAMTS9, restricted to the cell surface, and not processed to maturity. ADAMTS9-GT zymogen is likely to be proteolytically active (Koo et al., 2007), but its cell-surface confinement and reduced cellular levels implied compromised function.

Adamts9^{Gt} is a hypomorphic allele

Adamts9$^{Gt/+}$ mice lacked a highly penetrant ocular anomaly identified in *Adamts9*$^{lacZ/+}$ mice (Koo et al., 2010), and *Adamts9*$^{Gt/Gt}$ mice, unlike *Adamts9*$^{LacZ/LacZ}$ and *Adamts9*$^{Del/Del}$ mice survived past gastrulation (E7.0). ADAMTS20, which has an identical domain structure as ADAMTS9, was previously shown to work cooperatively with it in palatogenesis and skin pigmentation (Enomoto, 2010; Silver, 2008). We introduced an *Adamts9*^{Gt} allele into *Adamts20*$^{Bt/Bt}$, a mutant with white spotting in the lumbar region (Rao et al., 2003) (Fig. S3A). Like *Adamts9*$^{LacZ/+}$*; Adamts20*$^{Bt/Bt}$ or *Adamts9*$^{Del/+}$*; Adamts20*$^{Bt/Bt}$ mice, these mice died at birth with cleft palate (Dubail et al., 2014; Enomoto, 2010), and lacked skin melanoblasts (Silver, 2008) (Fig. S3A-F). Thus, *Adamts9*^{Gt} is a hypomorphic allele functionally equivalent to an *Adamts9* null allele in genetic interactions with *Adamts20*^{Bt}.

Adamts9$^{Gt/Gt}$ embryos have impaired umbilical cord growth

Adamts9$^{Gt/+}$ intercrosses did not provide *Adamts9*$^{Gt/Gt}$ mice at birth or weaning (Table S1). A Mendelian proportion of *Adamts9*$^{Gt/Gt}$ embryos was obtained from E12.5-E14.5, but none survived past E15.5. *Adamts9*$^{Gt/Gt}$ embryos older than E11.5 had unusual proximity to the placenta, revealing short umbilical cords with minimal growth beyond from E11.5-E14.5, whereas the WT cords doubled their length over this period (Fig. 1B-C). Coupled with minimally reduced embryo and placenta weight (Fig. 1B, Fig. S3G), this implied loss of a specific function in the umbilical cord with intrauterine embryonic growth restriction (IUGR) as a sequel. Although placental size was comparable (Fig. 1B), the endothelium-lined fetal compartment of *Adamts9*$^{Gt/Gt}$ placenta consistently contained stacks of nucleated red blood cells after E12.5 (Fig. S3H-I'), suggesting impaired umbilical cord circulation and secondary IUGR of *Adamts9*$^{Gt/Gt}$ embryos after E11.5. E8.5 to E12.5 *Adamts9*$^{LacZ/+}$ conceptuses were obtained by crossing WT females with *Adamts9*$^{LacZ/+}$ males, to bypass β-gal staining arising in maternal tissues. *Adamts9* was expressed in the umbilical cord

Author Manuscript Author Manuscript Author Manuscript Author Manuscript

insertion sites in the embryo (Fig. 1D-D'), and placenta (Fig. 1I-J) comprising Wharton's jelly transition zones. β-gal staining was strongest in the adventitia of the umbilical vessels, Wharton's jelly mesenchyme and endothelial cells of the umbilical vein but not arteries, whereas vascular smooth muscle cells (VSMCs) were unstained (Fig. 1E-H). An ADAMTS9 antibody is presently unavailable to investigate protein distribution.

VSMC orthogonal orientation is impaired in *Adamts9*$^{Gt/Gt}$ umbilical cords

By E14.5, WT umbilical cord mesenchyme formed two distinct layers around each artery (Fig. 1K), namely a 6-12 cells-thick zone of longitudinally oriented tunica adventitia cells, and an outer zone of randomly oriented and sparse mesenchymal cells (Wharton's jelly mesenchyme). In E14.5 WT arterial and venous walls, VSMCs were oriented orthogonally to adventitial cells i.e., circumferentially with respect to the lumen (Fig. 1K, M-N). Strikingly, VSMCs of E14.5 *Adamts9*$^{Gt/Gt}$ umbilical vessels were co-aligned with adventitial cells (Fig. 1L, O-P). By E14.5, both the VSMC and adventitia of the mutant umbilical vessels were less densely populated than WT umbilical vessels (Fig. 1L, O-P).

At E11.5, the *Adamts9*$^{Gt/Gt}$ umbilical vessel walls resembled the WT (Fig. 1Q-R), i.e., umbilical arteries comprised 1-2 layers of co-aligned VSMCs and adventitial cells. Thus, WT VSMCs, which are longitudinally oriented at E11.5, reorient orthogonally by E14.5 (Fig. 1K,Q), as previously observed in the pulmonary artery (Greif et al., 2012). In contrast, *Adamts9*$^{Gt/Gt}$ VSMCs fail to undergo reorientation (Fig. 1R,L).

Loss of ADAMTS9 function alters ECM dynamics and reduces VSMC proliferation

After E12.5, when umbilical vessel growth accelerates, *Adamts9*$^{Gt/Gt}$ umbilical vessels had fewer VSMC layers and narrower lumina, indicating impaired radial expansion (Fig. 2A, F). We observed reduced cellularity and increased intercellular spacing of VSMC and Wharton's jelly cells in *Adamts9*$^{Gt/Gt}$ umbilical cords (Fig. 2A). Transmission electron microscopy (TEM) identified overabundant amorphous, non-fibrillar interstitial ECM (Fig. 2B), although collagen fibril morphology was unaltered and *Adamts9*$^{Gt/Gt}$ umbilical cord VSMC had abundant organelles (Fig. S4A-B). Phospho-histone H3 (pHH3) staining showed fewer proliferating cells in mutant umbilical vessels (Fig. 2C-D, Fig. S4C-D) and cleaved caspase-3 staining revealed minimal cell death in both WT and mutant umbilical cords (Fig. 2E, Fig. S4E-F).

Versican, an ADAMTS9 substrate, forms aggregates with hyaluronan in Wharton's jelly (Gogiel et al., 2003). A polyclonal antibody against the versican GAG-β domain (present in splice isoforms V0 and V1) detected versican in the umbilical vascular wall and Wharton's jelly (Fig. 2G-H). Versican proteolysis (detected by a neo-epitope antibody to-DPEAAE^{441}) (Sandy et al., 2001) was detectable in WT umbilical cords but not in *Adamts9*$^{Gt/Gt}$ mutants (Fig. 2I-J). In the WT placenta, versican and DPEAAE staining coincided with *Adamts9* expression and there was less cleaved versican in the *Adamts9*$^{Gt/Gt}$ mutant (Fig. S4H-K). Endomucin labeled the labyrinth vessels, which were morphologically similar between WT and mutant placentas (Fig. S4H-K). Hyaluronan-binding protein (HAbp) staining of umbilical cords was unaltered (Fig. 2K-L), but fibronectin and fibrillin-2, typical provisional matrix constituents, showed enhanced staining in *Adamts9*$^{Gt/Gt}$ umbilical vessels (Fig. 2M-

Author Manuscript Author Manuscript Author Manuscript Author Manuscript

P'). Elastin is normally present in a non-laminar pattern surrounding individual VSMCs in the embryonic mouse aorta (Wagenseil and Mecham, 2009), similar to its distribution in WT umbilical cord SMCs at E12.5, and was decreased in the mutant vessels (Fig. 2Q-R'), but collagen IV staining was comparable (Fig. 2S-T'). The filamentous actin (F-actin) network and F-actin-interacting contractile proteins drive cell shape changes during morphogenesis (Nandadasa et al., 2009). Phalloidin and phosphorylated myosin light chain (pMLC) staining indicating the F-actin network and contractility competence respectively, were greatly reduced in *Adamts9*$^{Gt/Gt}$ VSMCs (Fig. 2U-X). αSMA immunofluorescence revealed significantly lower staining intensity in mutant VSMCs (Fig. 4A-B'). Collectively, these findings point to severe impairment of *Adamts9*$^{Gt/Gt}$ VSMC differentiation.

Altered ECM dynamics attenuates Shh and PDGFR-β signaling in the umbilical vascular wall

Shh signaling is critical for VSMC differentiation in the dorsal aorta, and is required for investment by multiple VSMC layers (Passman et al., 2008). Strong expression of Shh, Patched-1, and Gli-1 was previously seen in the umbilical cord at E13.5 but not E11.5 (Haraguchi et al., 2007). In *del5*-LacZ mice, which report Hh signaling, β-gal staining in the umbilical cord was observed from E12.0 (Haraguchi et al., 2007). We observed strong Shh staining in the tunica media of E12.5 WT but not mutant umbilical vessels (Fig. 3C-D'). Gli-1, a reporter of Shh signaling activity, and Sca-1, a marker of the progenitor state maintained by Shh signaling (Passman et al., 2008), were reduced in *Adamts9*$^{Gt/Gt}$ umbilical vessels (Fig. 3E-H). The PDGFR-β signaling pathway is critical for recruitment of VSMC and pericytes by endothelial cells (Armulik et al., 2011) and *Pdgfb*$^{-/-}$ embryos have short umbilical cords (Hellstrom et al., 1999). PDGFR-β signaling activates Shh during vascular maturation (Yao et al., 2014), and was implicated in radial growth and SMC reorientation during pulmonary arterial wall development (Greif et al., 2012). PDGF-B, the ligand for PDGFRβ, is produced by vascular endothelial cells and contains a C-terminal ECM retention motif (Andrae et al., 2008), which interacts with heparin-sulfate proteoglycans. We observed strong PDGFRβ expression in juxta-endothelial VSMC in WT umbilical vessels, whereas mutant umbilical vessels showed reduced expression (Fig. 3I-J'). Phosphorylated-ERK1/2 staining, reporting PDGFR-β signaling, among other pathways, revealed a lack of activation of the ERK/MAPK pathway in mutant VSMC (Fig. 3K-L). Since the ERK/MAPK pathway is a major regulator of cytoskeletal dynamics in many cell types (Kolch, 2005), this may explain the reduced actin cytoskeleton and impaired orthogonal rotation in the mutant VSMC. Thus, two major pathways regulating VSMC recruitment and differentiation, i.e., Shh and PDGFR-β pathways, are active during normal umbilical cord development and compromised in *Adamts9*$^{Gt/Gt}$ cords.

The preferred radial orientation of cilia is disrupted in *Adamts9*$^{Gt/Gt}$ umbilical cord mesenchyme

Primary cilia are cellular organelles projecting into the microenvironment that are implicated in Shh, PDGFRα, and Wnt signaling (Fliegauf et al., 2007). They may work as ECM sensors in connective tissues (Donnelly et al., 2008; McGlashan et al., 2006), since ECM molecules such as collagens and proteoglycans interact with the cilium membrane (Jensen et al., 2004). Integrins α3, α5, and β1 localize to the primary cilium of aortic VSMCs, and

Author Manuscript Author Manuscript Author Manuscript Author Manuscript

were implicated in fibronectin–induced Ca^{+2} signaling (Lu et al., 2008; McGlashan et al., 2006; Praetorius et al., 2004). Confocal Z-stack projections of WT umbilical cords stained with acetylated tubulin revealed primary cilia in most mesenchymal and mesothelial cells, but not vascular endothelium (Fig. 4A-D). Most umbilical VSMCs lacked primary cilia (Fig. 4A), contrasting with cilia reported in adult mouse aortic VSMCs (Lu et al., 2008). Primary cilia in the adventitium and Wharton's jelly of WT umbilical cords had a preferred radial orientation, whereas *Adamts9*$^{Gt/Gt}$ umbilical cords had a high percentage of cells whose cilia veered away from this orientation (arrowheads in Fig. 4A',B'). Radar plots of the minor angle of individual cilia to a radial vector showed that WT cells had an average cilia angle of 36.95 degrees whilst mutant cells had an average angle of 56.08 degrees (Fig. 4 E). Integrins β1 and α5 co-localized with some umbilical cord mesenchymal cilia (Fig. 4F), supporting a cilium-ECM interaction. Thus, altered ECM dynamics in the mutant umbilical cord is not only accompanied by compromised Shh signaling, but altered orientation of the primary cilium, a key participant in the pathway (Goetz and Anderson, 2010).

Tbx4-Cre mediated conditional deletion of *Adamts9,* but not VSMC-specific deletion, recapitulates the *Adamts9*$^{Gt/Gt}$ defect

Conditional deletion of *Adamts9* using *Tbx4*-Cre, which is expressed in the developing hind limbs, lung mesenchyme, and the umbilical cord mesenchyme, but not in the embryonic heart or yolk sac in mice (Greif et al., 2012; Naiche et al., 2011) embryos led to significantly shorter umbilical cords than *Adamts9*$^{Fl/+}$ and *Tbx4*-Cre; *Adamts9*$^{Fl/+}$ siblings by E12.5 (Fig. S5A C). A dual tomato reporter showed that *Tbx4*-Cre expression overlapped substantially with *Adamts9* in the adventitia (Fig. S5D-G) but not Wharton's jelly mesenchyme or vascular endothelium (Fig. S5E-F). Impairment of VSMC rotation in *Tbx4*-Cre conditionally deleted umbilical cords was seen, but was less severe than in *Adamts9*$^{Gt/Gt}$ umbilical cords (Fig. S5H M), consistent with spatially limited deletion by *Tbx4*-Cre, and did not impair embryo survival. Conditional deletion by *Tagln*-Cre, did not impair embryonic survival or umbilical cord growth (Fig. S5N-P) since deletion occurred only in VSMC, but not most cells expressing ADAMTS9 (Fig. S5Q-S), and had no impact on VSMC rotation (Fig. S5T-Y). Thus, ADAMTS9 secreted by adventitial cells and mesenchyme influences VSMCs non-autonomously during umbilical vessel development.

A proposed role for ADAMTS9-mediated ECM dynamics in umbilical cord VSMC differentiation

We show that the murine umbilical cord undergoes rapid growth, along with longitudinal and radial growth of umbilical vessels after 11.5 days of gestation. Umbilical arteries acquire 3-4 layers of VSMC by E14.5, with 1-2 layers constituting the corresponding venous wall. Around E12.5, after commitment to the SMC lineage and acquisition of SMA expression, the VSMCs reorient orthogonally (i.e. rotate), proliferate, and begin to build a vascular matrix containing elastin. Wharton's jelly mesenchyme remains undifferentiated throughout, and contains abundant ECM. Between Wharton's jelly and VSMCs, a *de facto* adventitia comprising closely packed, longitudinally oriented cells is formed. Primary cilia, found here, and in the mesenchymal and mesothelial cells of the umbilical cord are normally radially oriented. This umbilical cord vasculature organization (Fig. 5A) appears to be maintained through further development.

Author Manuscript Author Manuscript Author Manuscript Author Manuscript

Upon secretion, ADAMTS9 localizes to the cell surface, presumably binding to pericellular matrix or cell-surface proteins, where it is processed by furin, but it is also released from cells and detectable in their medium (Koo et al., 2006, 2007). Unimpaired normal gastrulation in *Adamts9*$^{Gt/Gt}$ embryos, yet impeded later development (including cooperative functions with *Adamts20*), suggests existence of two functional pools of ADAMTS9 (Fig. 5B). The cell-proximate pool, i.e. pericellular ADAMTS9, albeit at lower levels in ADAMTS9-GT, suffices where ECM resides close to the cell surface (such as in the gastrulating embryo). In contrast, the secreted or "cell-distal" pool, shown to be lacking in ADAMTS9-GT transfected cells, acts at longer range and non-cell-autonomously and is crucial where interstitial ECM is abundant (Fig. 5B). We propose that long-range ADAMTS9 activity becomes increasingly necessary with enhanced interstitial ECM as embryogenesis progresses.

We show that VSMC specialization, including orthogonal reorientation, requires proper ECM dynamics mediated by ADAMTS9 acting non-autonomously in the umbilical cord. Mechanistically, ECM interactions of Shh and PDGF-BB are critical for their normal function (Stenzel et al., 2009; Varjosalo and Taipale, 2008) and could be impaired by altered ECM dynamics, which may affect their release or transport. Altered ECM composition and density could also affect cilium orientation, as shown here, and directly impair Shh signaling (Fig. 5B). We propose that activation of the MAPK/ERK pathway in VSMCs in response to PDGFR-β and other signaling inputs may regulate cytoskeletal dynamics required for VSMC reorientation (Fig. 5B). Indeed, in *Adamts9*$^{Gt/Gt}$ umbilical cords, F-actin, smooth muscle α-actin, and phosphorylated MLC staining were dramatically reduced, and the final effect of the altered ECM dynamics would be to compromise cell rotation through these cytoskeletal changes potentially coupled with impedance by enhanced pericellular matrix.

Experimental procedures

Transgenic mice and genotyping

R1 male embryonic stem cells with insertion of UPATrap at the *Adamts9* locus were injected into blastocysts and chimeras were bred to WT mice for germline transmission of the trapped allele. *Adamts9*$^{LacZ/+}$ (Kern et al., 2010), and the *Adamts20* mutant *Adamts20*$^{\text{bt-Bei1}}$ (referred to as *Adamts20*^{Bt}) (Rao et al., 2003; Silver, 2008) were described previously. Germline deletion of *Adamts9*$^{\text{fl}}$ (RRID:JAX_026103) provided the *Adamts9*$^{\text{Del}}$ allele (Dubail et al., 2014). *Adamts*$^{\text{fl}}$ mice were crossed extensively with *ROSA*$^{\text{mT/mG}}$ reporter mice (Muzumdar et al., 2007) to achieve linkage of the two transgenes on chr 6. *Tbx4*-Cre (Naiche et al., 2011), and *Tagln*-Cre (Holtwick et al., 2002) strains were used for *Adamts9*$^{\text{fl}}$ conditional deletion. Additional details are provided in Supplemental methods.

Embryo analysis

Paraformaldehyde-fixed tissue was embedded in ultrapure agarose and vibratome-sectioned, or embedded in paraffin for sectioning. Analysis of sections by immunofluorescence or fluorescence microscopy, ascertainment of primary cilium orientation, and transmission electron microscopy is described in Supplemental methods.

Author Manuscript Author Manuscript Author Manuscript Author Manuscript

Molecular cloning, cell and biochemical analysis

Determination of the UPATrap insertion site, generation of plasmids expressing truncated ADAMTS9, molecular cloning of ADAMTS9 splice variants, cell culture, transfection, biotinylation and western blotting is described in Supplemental methods.

Supplementary Material

Refer to Web version on PubMed Central for supplementary material.

Acknowledgements

We thank Ron Conlon and the CWRU Transgenic Core for generating *Adamts9*^{Gt} mice, Naiche Adler for *Tbx4*-Cre mice, and Elliot Philipson for helpful discussion.

Funding: This work was supported by NIH awards HL107147 and HD067947 to SA, a Morgenthaler fellowship to SN, and by Sabrina's Foundation.

References

Andrae J, Gallini R, Betsholtz C. Role of platelet-derived growth factors in physiology and medicine. Genes Dev. 2008; 22:1276–1312. [PubMed: 18483217]

Apte SS. A disintegrin-like and metalloprotease (reprolysin-type) with thrombospondin type 1 motif (ADAMTS) superfamily: functions and mechanisms. J Biol Chem. 2009; 284:31493–31497. [PubMed: 19734141]

Armulik A, Genove G, Betsholtz C. Pericytes: developmental, physiological, and pathological perspectives, problems, and promises. Dev Cell. 2011; 21:193–215. [PubMed: 21839917]

Benirschke, K.; B.G.J.; Baergen, RN. Pathology of the Human Placenta. Springer-Verlag; Berlin Heidelberg: 2012. Anatomy and Pathology of the Umbilical Cord; p. 309-376.

Blelloch R, Anna-Arriola SS, Gao D, Li Y, Hodgkin J, Kimble J. The gon-1 gene is required for gonadal morphogenesis in Caenorhabditis elegans. Dev Biol. 1999; 216:382–393. [PubMed: 10588887]

Bonnans C, Chou J, Werb Z. Remodelling the extracellular matrix in development and disease. Nature reviews Molecular cell biology. 2014; 15:786–801.

Camenisch TD, Spicer AP, Brehm-Gibson T, Biesterfeldt J, Augustine ML, Calabro A Jr. Kubalak S, Klewer SE, McDonald JA. Disruption of hyaluronan synthase-2 abrogates normal cardiac morphogenesis and hyaluronan-mediated transformation of epithelium to mesenchyme. J Clin Invest. 2000; 106:349–360. [PubMed: 10930438]

Donnelly E, Williams R, Farnum C. The primary cilium of connective tissue cells: imaging by multiphoton microscopy. Anat Rec. 2008; 291:1062–1073.

Dubail J, Aramaki-Hattori N, Bader HL, Nelson CM, Katebi N, Matuska B, Olsen BR, Apte SS. A new Adamts9 conditional mouse allele identifies its non-redundant role in interdigital web regression. Genesis. 2014; 52:702–712. [PubMed: 24753090]

Dupuis LE, McCulloch DR, McGarity JD, Bahan A, Wessels A, Weber D, Diminich AM, Nelson CM, Apte SS, Kern CB. Altered versican cleavage in ADAMTS5 deficient mice; a novel etiology of myxomatous valve disease. Dev Biol. 2011; 357:152–164. [PubMed: 21749862]

Enomoto H, Nelson C, Somerville RPT, Mielke K, Dixon L, Powell K, Apte SS. Cooperation of two ADAMTS metalloproteases in closure of the mouse palate identifies a requirement for versican proteolysis in regulating palatal mesenchyme proliferation. Development. 2010; 137:4029–4038. [PubMed: 21041365]

Fliegauf M, Benzing T, Omran H. When cilia go bad: cilia defects and ciliopathies. Nature reviews Molecular cell biology. 2007; 8:880–893.

Goetz SC, Anderson KV. The primary cilium: a signalling centre during vertebrate development. Nat Rev Genet. 2010; 11:331–344. [PubMed: 20395968]

Author Manuscript Author Manuscript Author Manuscript Author Manuscript

Gogiel T, Bankowski E, Jaworski S. Proteoglycans of Wharton's jelly. Int J Biochem Cell Biol. 2003; 35:1461–1469. [PubMed: 12818241]

Greif DM, Kumar M, Lighthouse JK, Hum J, An A, Ding L, Red-Horse K, Espinoza FH, Olson L, Offermanns S, et al. Radial construction of an arterial wall. Dev Cell. 2012; 23:482–493. [PubMed: 22975322]

Haraguchi R, Motoyama J, Sasaki H, Satoh Y, Miyagawa S, Nakagata N, Moon A, Yamada G. Molecular analysis of coordinated bladder and urogenital organ formation by Hedgehog signaling. Development. 2007; 134:525–533. [PubMed: 17202190]

Hellstrom M, Kalen M, Lindahl P, Abramsson A, Betsholtz C. Role of PDGF-B and PDGFR-beta in recruitment of vascular smooth muscle cells and pericytes during embryonic blood vessel formation in the mouse. Development. 1999; 126:3047–3055. [PubMed: 10375497]

Holtwick R, Gotthardt M, Skryabin B, Steinmetz M, Potthast R, Zetsche B, Hammer RE, Herz J, Kuhn M. Smooth muscle-selective deletion of guanylyl cyclase-A prevents the acute but not chronic effects of ANP on blood pressure. Proc Natl Acad Sci U S A. 2002; 99:7142–7147. [PubMed: 11997476]

Ismat A, Cheshire AM, Andrew DJ. The secreted AdamTS-A metalloprotease is required for collective cell migration. Development. 2013; 140:1981–1993. [PubMed: 23536567]

Jensen CG, Poole CA, McGlashan SR, Marko M, Issa ZI, Vujcich KV, Bowser SS. Ultrastructural, tomographic and confocal imaging of the chondrocyte primary cilium in situ. Cell Biol Int. 2004; 28:101–110. [PubMed: 14984755]

Kern CB, Wessels A, McGarity J, Dixon LJ, Alston E, Argraves WS, Geeting D, Nelson CM, Menick DR, Apte SS. Reduced versican cleavage due to Adamts9 haploinsufficiency is associated with cardiac and aortic anomalies. Matrix Biol. 2010; 29:304–316. [PubMed: 20096780]

Kolch W. Coordinating ERK/MAPK signalling through scaffolds and inhibitors. Nature reviews Molecular cell biology. 2005; 6:827–837.

Koo BH, Coe DM, Dixon LJ, Somerville RP, Nelson CM, Wang LW, Young ME, Lindner DJ, Apte SS. ADAMTS9 Is a Cell-Autonomously Acting,Anti-Angiogenic Metalloprotease Expressed by Microvascular Endothelial Cells. Am J Pathol. 2010

Koo BH, Longpre JM, Somerville RP, Alexander JP, Leduc R, Apte SS. Cell-surface processing of pro-ADAMTS9 by furin. J Biol Chem. 2006; 281:12485–12494. [PubMed: 16537537]

Koo BH, Longpre JM, Somerville RP, Alexander JP, Leduc R, Apte SS. Regulation of ADAMST9 secretion and enzymatic activity by its propeptide. J Biol Chem. 2007; 282:16146–16154. [PubMed: 17403680]

Kwon GS, Viotti M, Hadjantonakis AK. The endoderm of the mouse embryo arises by dynamic widespread intercalation of embryonic and extraembryonic lineages. Dev Cell. 2008; 15:509–520. [PubMed: 18854136]

Lu CJ, Du H, Wu J, Jansen DA, Jordan KL, Xu N, Sieck GC, Qian Q. Non-random distribution and sensory functions of primary cilia in vascular smooth muscle cells. Kidney Blood Press Res. 2008; 31:171–184. [PubMed: 18483460]

McCulloch DR, Nelson CM, Dixon LJ, Silver DL, Wylie JD, Lindner V, Sasaki T, Cooley MA, Argraves WS, Apte SS. ADAMTS metalloproteases generate active versican fragments that regulate interdigital web regression. Dev Cell. 2009; 17:687–698. [PubMed: 19922873]

McGlashan SR, Jensen CG, Poole CA. Localization of extracellular matrix receptors on the chondrocyte primary cilium. J Histochem Cytochem. 2006; 54:1005–1014. [PubMed: 16651393]

Miner JH, Li C, Mudd JL, Go G, Sutherland AE. Compositional and structural requirements for laminin and basement membranes during mouse embryo implantation and gastrulation. Development. 2004; 131:2247–2256. [PubMed: 15102706]

Mouw JK, Ou G, Weaver VM. Extracellular matrix assembly: a multiscale deconstruction. Nature reviews Molecular cell biology. 2014; 15:771–785.

Muzumdar MD, Tasic B, Miyamichi K, Li L, Luo L. A global double-fluorescent Cre reporter mouse. Genesis. 2007; 45:593–605. [PubMed: 17868096]

Naiche LA, Arora R, Kania A, Lewandoski M, Papaioannou VE. Identity and fate of Tbx4-expressing cells reveal developmental cell fate decisions in the allantois, limb, and external genitalia. Dev Dyn. 2011; 240:2290–2300. [PubMed: 21932311]

Author Manuscript Author Manuscript Author Manuscript Author Manuscript

Nandadasa S, Tao Q, Menon NR, Heasman J, Wylie C. N- and E-cadherins in Xenopus are specifically required in the neural and non-neural ectoderm, respectively, for F-actin assembly and morphogenetic movements. Development. 2009; 136:1327–1338. [PubMed: 19279134]

Naso MF, Morgan JL, Buchberg AM, Siracusa LD, Iozzo RV. Expression pattern and mapping of the murine versican gene (Cspg2) to chromosome 13. Genomics. 1995; 29:297–300. [PubMed: 8530092]

Passman JN, Dong XR, Wu SP, Maguire CT, Hogan KA, Bautch VL, Majesky MW. A sonic hedgehog signaling domain in the arterial adventitia supports resident Sca1+ smooth muscle progenitor cells. Proc Natl Acad Sci U S A. 2008; 105:9349–9354. [PubMed: 18591670]

Peters JH, Hynes RO. Fibronectin isoform distribution in the mouse. I. The alternatively spliced EIIIB, EIIIA, and V segments show widespread codistribution in the developing mouse embryo. Cell Adhes Commun. 1996; 4:103–125. [PubMed: 8937746]

Praetorius HA, Praetorius J, Nielsen S, Frokiaer J, Spring KR. Beta1-integrins in the primary cilium of MDCK cells potentiate fibronectin-induced Ca2+ signaling. American journal of physiology Renal physiology. 2004; 287:F969–978. [PubMed: 15226154]

Rao C, Foernzler D, Loftus SK, Liu S, McPherson JD, Jungers KA, Apte SS, Pavan WJ, Beier DR. A defect in a novel ADAMTS family member is the cause of the belted white-spotting mutation. Development. 2003; 130:4665–4672. [PubMed: 12925592]

Sandy JD, Westling J, Kenagy RD, Iruela-Arispe ML, Verscharen C, Rodriguez-Mazaneque JC, Zimmermann DR, Lemire JM, Fischer JW, Wight TN, et al. Versican V1 proteolysis in human aorta in vivo occurs at the Glu441-Ala442 bond, a site that is cleaved by recombinant ADAMTS-1 and ADAMTS-4. The Journal of biological chemistry. 2001; 276:13372–13378. [PubMed: 11278559]

Silver DL, Hou L, Somerville R, Young ME, Apte SS, Pavan WJ. The secreted metalloprotease ADAMTS20 is required for melanoblast survival. PLoS Genet. 2008; 4:1–15.

Sobolewski K, Bankowski E, Chyczewski L, Jaworski S. Collagen and glycosaminoglycans of Wharton's jelly. Biology of the neonate. 1997; 71:11–21. [PubMed: 8996653]

Stankunas K, Hang CT, Tsun ZY, Chen H, Lee NV, Wu JI, Shang C, Bayle JH, Shou W, Iruela-Arispe ML, et al. Endocardial Brg1 represses ADAMTS1 to maintain the microenvironment for myocardial morphogenesis. Dev Cell. 2008; 14:298–311. [PubMed: 18267097]

Stenzel D, Nye E, Nisancioglu M, Adams RH, Yamaguchi Y, Gerhardt H. Peripheral mural cell recruitment requires cell-autonomous heparan sulfate. Blood. 2009; 114:915–924. [PubMed: 19398718]

Stupka N, Kintakas C, White JD, Fraser FW, Hanciu M, Aramaki-Hattori N, Martin S, Coles C, Collier F, Ward AC, et al. Versican processing by a disintegrin-like and metalloproteinase domain with thrombospondin-1 repeats proteinases-5 and -15 facilitates myoblast fusion. J Biol Chem. 2013; 288:1907–1917. [PubMed: 23233679]

Varjosalo M, Taipale J. Hedgehog: functions and mechanisms. Genes Dev. 2008; 22:2454–2472. [PubMed: 18794343]

Wagenseil JE, Mecham RP. Vascular extracellular matrix and arterial mechanics. Physiol Rev. 2009; 89:957–989. [PubMed: 19584318]

Yao Q, Renault MA, Chapouly C, Vandierdonck S, Belloc I, Jaspard-Vinassa B, Daniel-Lamaziere JM, Laffargue M, Merched A, Desgranges C, et al. Sonic hedgehog mediates a novel pathway of PDGF-BB-dependent vessel maturation. Blood. 2014; 123:2429–2437. [PubMed: 24472833]

Author Manuscript Author Manuscript Author Manuscript Author Manuscript

Highlights

Cell-membrane ADAMTS9 suffices for gastrulation, but not for later mouse development.

ADAMTS9 is required for versican proteolysis during umbilical cord vascular growth.

Extracellular matrix accumulation impairs umbilical smooth muscle differentiation.

Matrix dynamics regulates primary cilium orientation, and Shh and PDGFRb signaling.

Author Manuscript Author Manuscript Author Manuscript Author Manuscript

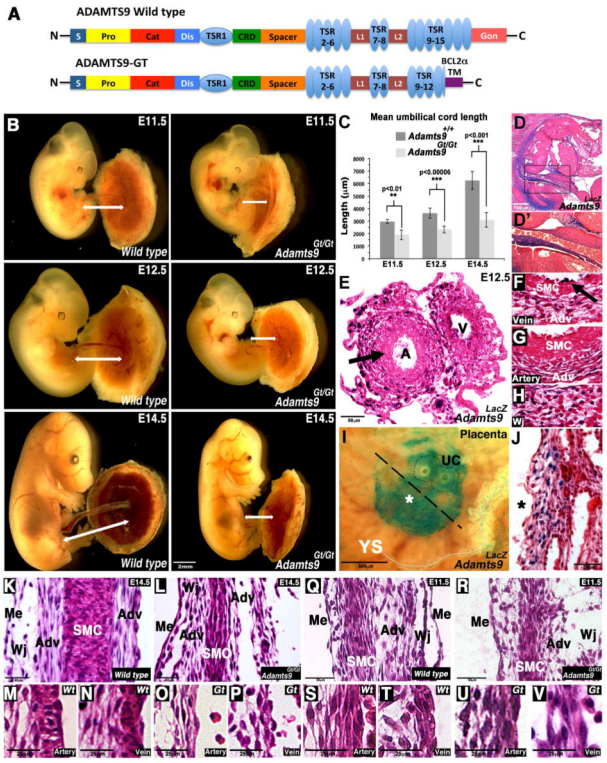

Figure 1. An *Adamts9* gene trap impairs umbilical cord development

(A) Schematic of WT ADAMTS9 and ADAMTS9-GT (S, signal peptide; Pro, propeptide; Cat, catalytic domain; Dis, Disintegrin-like module; TSR, Thrombospondin type 1 repeat; CRD, cysteine rich module; L1-L2, linkers 1-2; TM, Transmembrane domain). **(B)** *Adamts9*$^{Gt/Gt}$ embryos have short umbilical cords (arrows). **(C)** WT, but not *Adamts9*$^{Gt/Gt}$ umbilical cords double in length between E11.5-E14.5 (n=7 cords for each group at E12.5, n=3 cords for each group at E11.5, and E14.5. Error bars= S.D. p values determined by Student's t test). **(D-D')** βgal and eosin staining of E12.5 *Adamts9*$^{LacZ/+}$ embryo showing *Adamts9* expression (blue) at the embryo umbilical cord insertion site (arrow). **(E-H)** Cross sections of E12.5 *Adamts9*$^{LacZ/+}$ umbilical cord showing *Adamts9* expression (blue) in adventitia, Wharton's jelly, and venous endothelium. Arrow in E indicates the tunica media. **F-H** show higher magnification of the umbilical vein, artery and Wharton's jelly. Black arrow in **F** shows *Adamts9* expression in the venous endothelium. **(I-J)** *En face* view of E12.5 *Adamts9*$^{LacZ/+}$ placenta shows β-gal staining at the umbilical cord insertion site. The dotted line circles umbilical vessels. Dashed line indicates the section plane in **J**, showing *Adamts9* expression is confined to Wharton's jelly at the umbilical cord insertion site. **(K-P)** Hematoxylin and eosin stained sagittal sections of E14.5 WT **(K, M-N)** and *Adamts9*$^{Gt/Gt}$ **(L, O-P)** umbilical cords. In **K** and **L,** sections are tangential through the tunica media of the umbilical artery. In **M-P,** sections are taken through the lumina. WT SMCs are aligned orthogonal to adventitial cells and the endothelium, but *Adamts9*$^{Gt/Gt}$ SMCs are fewer and co-aligned with adventitial cells. **(Q-R)** At E11.5, both WT **(Q, S-T)** and *Adamts9*$^{Gt/Gt}$ **(R, U-V)** VSMC are co-aligned with adventitial cells. **Q** and **R** show tangential sections through the tunica media of the umbilical artery, **S-V** are through the lumina. Scale bars= 2mm in **B**,

100μm in **D**, 50μm in **E**, 500μm in **I**, 25μm in **J**, 50μm in **K-L, Q-R**, 25μm in **M N**, **O-P, S-T, U-V**. Me, mesothelium; Wj, Wharton's jelly; Adv, adventitia. See also, Figs S1-3, S5 and Table S1.

Author Manuscript Author Manuscript Author Manuscript Author Manuscript

Author Manuscript Author Manuscript Author Manuscript Author Manuscript

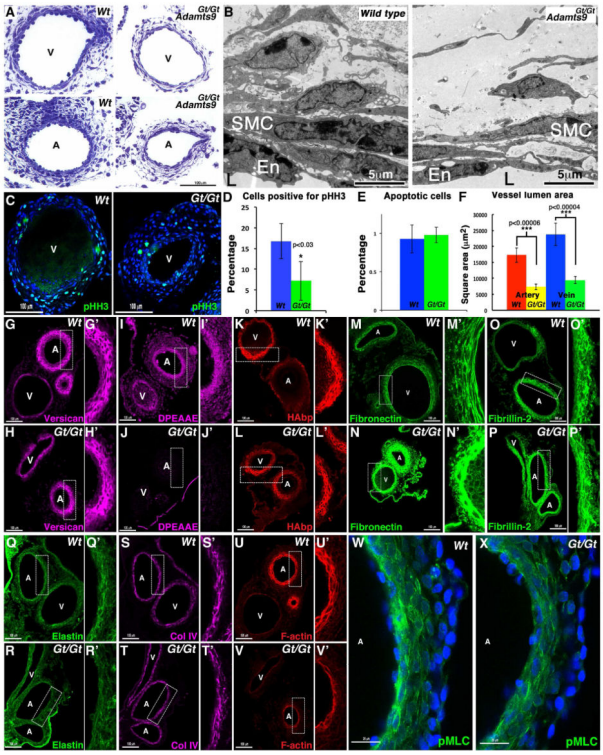

Figure 2. ADAMTS9 is required for umbilical cord VSMC growth and ECM homeostasis

(A) Toluidine blue staining of E12.5 WT and *Adamts9*$^{Gt/Gt}$ umbilical cords shows smaller, thinner-walled vessels in the mutant. **(B)** TEM of WT and *Adamts9*$^{Gt/Gt}$ umbilical vein shows increased amorphous ECM in the mutant. **(C-D)** Phospho-Histone H3 (pHH3) staining in umbilical vein shows reduced cell proliferation in the mutant (n=4 cords for each group. Error bars= S.D. p values determined by Student's t test). **(E)** Comparable numbers of cleaved caspase-3 stained cells were seen in WT and mutant umbilical cords (n=3 cords for each group. Error bars, S.D. p values determined by Student's t test). **(F)** *Adamts9*$^{Gt/Gt}$ umbilical vessels show significantly smaller lumenal areas than WT vessels (n=5 cords for each group. Error bars, S.E.M. p values determined by Student's t test). **(G-J)** Immunostaining for versican (GAGβ) demonstrates versican in both WT and *Adamts9*$^{Gt/Gt}$ umbilical vessels (**G-H)**, but cleaved versican (anti-DPEAAE) is present only in WT umbilical cord. **(K-L)** Hyaluronan-binding protein (HAbp) staining was comparable in WT and mutant cords. **(M-P)** Fibronectin **(M-N)**, and fibrillin-2 **(O-P)** immunostaining demonstrated stronger staining in *Adamts9*$^{Gt/Gt}$ umbilical vessels. **(Q-R)** Elastin immunostaining showed a non-laminar staining pattern in WT umbilical vessels and weaker staining in the mutant. **(S-T) C**ollagen-IV antibody comparably stained WT and *Adamts9*$^{Gt/Gt}$ umbilical cords. **(U-X)** Phalloidin **(U,V)** and phosphorylated MLC staining **(W,X)** demonstrated an attenuated cytoskeletal network and suggested reduced contractility in the *Adamts9*$^{Gt/Gt}$ VSMCs. Boxed areas are illustrated at higher magnification in **G'-V'**. A, artery; V, vein; SMC, smooth muscle cell; En, endothelium. Scale bars= 100μm in **A,C, G-V**, 25μm in W-X**,** and 5μm in **B.** See also Fig. S4.

Author Manuscript Author Manuscript Author Manuscript Author Manuscript

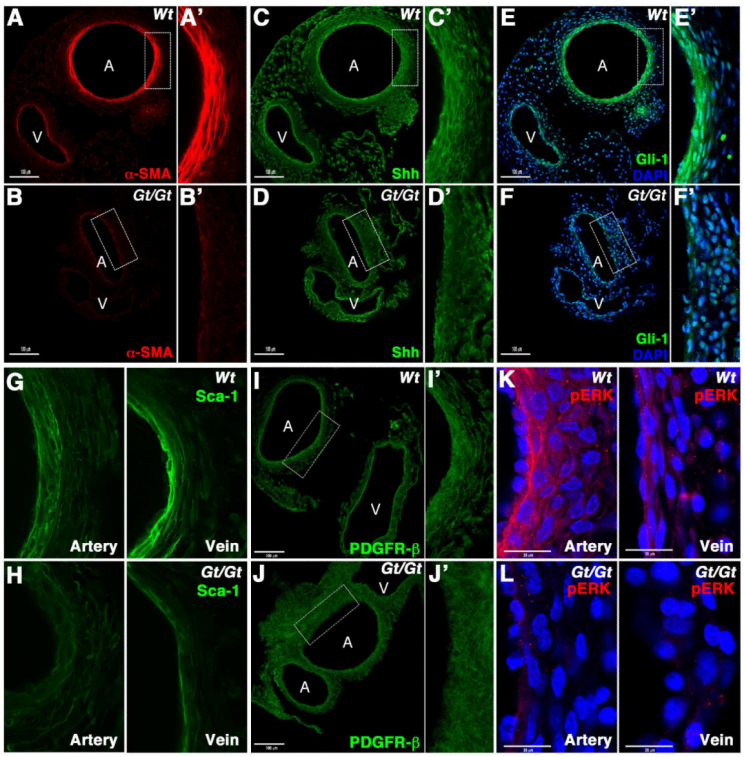

Figure 3. Dysregulated Shh and PDGF-B signaling in *Adamts9*$^{Gt/Gt}$ umbilical cords

(A-B). Strong α-SMA staining of VSMC in E12.5 WT, but not *Adamts9*$^{Gt/Gt}$ umbilical vessels. Magnified images of the arterial wall are illustrated in **A'** and **B'**. **(C-F)** Shh **(C-D)** and Gli-1 **(E-F)** immunostaining was weaker in the *Adamts9*$^{Gt/Gt}$ umbilical vessels. Boxed areas are illustrated at higher magnification in **C'-F'**. **(G-H**) Sca-1 is localized to the innermost VSMC layer in the WT umbilical artery and vein, but has reduced intensity in the mutant. **(I-L)** Immunostaining for PDGFRβ **(I-J)** and pERK1/2 **(K-L)** in WT and mutant umbilical cords, shows weak staining for PDGFRβ and no staining for pERK1/2 in the mutant. The boxed areas are illustrated at higher magnification in **I'-J'**. Scale bars= 100μm in **A-J**, 25μm in **K-L**.

Author Manuscript Author Manuscript Author Manuscript Author Manuscript

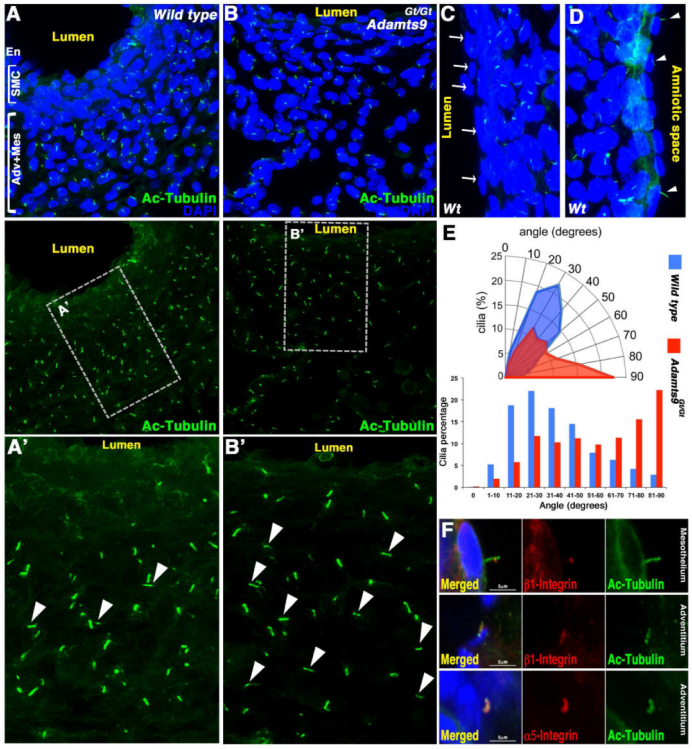

Figure 4. Primary cilium orientation is perturbed in *Adamts9*$^{Gt/Gt}$ umbilical cords

(A-D) Maximum intensity projections of confocal Z-sections from the arterial wall of E12.5 WT **(A-A')** and *Adamts9*$^{Gt/Gt}$ **(B-B')** umbilical cords stained with acetylated tubulin (green) and DAPI (blue). Note paucity of cilia in WT VSMC and high prevalence in mesenchyme. Arrowheads in **A'** and **B'** point to cilia oriented orthogonal to a radial vector in the *Adamts9*$^{Gt/Gt}$ vessels with fewer seen in WT. **(C-D)** Primary cilia are absent in vascular endothelium **(C,** arrows**)** but are present in the mesothelium **(D,** arrowheads**)**. **(E)** Measurement of minor angle of the cilium to a radial vector arising from the lumen of WT and mutant umbilical vessels, binned in 10° intervals (n=4 cords for each group). The radar-plot demonstrates that a high percentage of mutant cilia are misaligned. **(E)** Co-immunostaining for acetylated tubulin (green) and integrins βl and α5 (red) in WT umbilical cords shows that in some mesenchymal cells, integrins localized to cilia. Scale bars =100μm in **A-B**, 25μm in **C-D**, 5μm in **F**.

Author Manuscript Author Manuscript Author Manuscript Author Manuscript

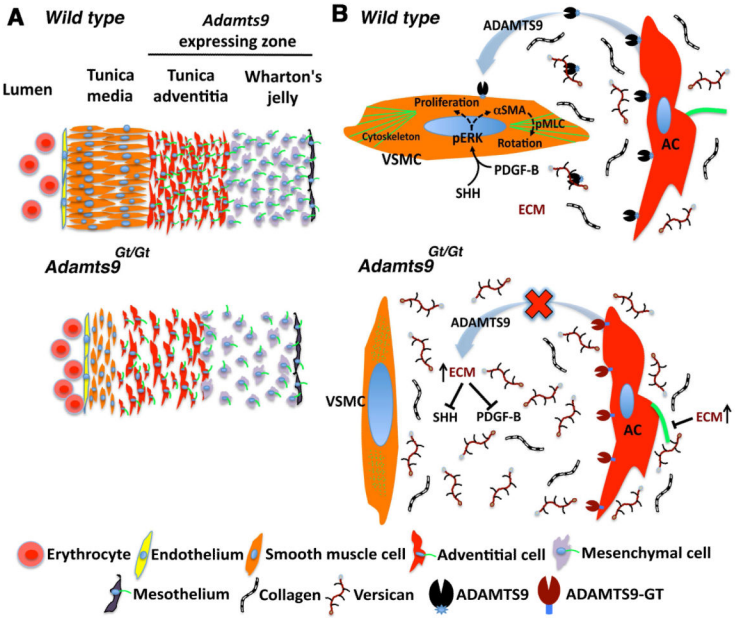

Figure 5. ADAMTS9-mediated ECM dynamics regulates VSMC development in the umbilical cord

(A) The normal umbilical vessel has three major layers. VSMCs are oriented orthogonal to adventitial cells, and primary cilia (green) have a preferred radial orientation, which is perturbed in the mutant **(B)** Two pools of ADAMTS9, pericellular and secreted (black) in adventitial and mesenchymal cells, cleave versican to facilitate ECM remodeling and enable normal Shh and PDGF-B signaling via ERK1/2 phosphorylation, which regulates VSMC differentiation. In *Adamts9*$^{Gt/Gt}$ ADAMTS9-GT (brown) is cell-surface restricted and versican turnover is reduced. Altered ECM dynamics may affect release and transport of Shh and PDGF-B, or act via ECM sensing by the cilium. Failed orthogonal rotation may result from reduced MAPK/ERK activation, an effete cytoskeleton, loss of p-MLC and αSMA, or physical impedance by accumulated pericellular ECM around *Adamts9*$^{Gt/Gt}$ VSMC. See also Fig. S5.